Journal of Materials Chemistry C

Tuning the Structural and Spectroscopic Properties of Donor-Acceptor-Donor Oligomers via Mutual X-Bonding, H-Bonding, and π-π Interactions

Journal:	*Journal of Materials Chemistry C*
Manuscript ID	TC-ART-01-2018-000074.R1
Article Type:	Paper
Date Submitted by the Author:	07-Mar-2018

Complete List of Authors:	Weldeab, Asmerom ; University of Florida, Department of Chemistry Steen, April; University of Mississippi, Chemistry and Biochemistry Starkenburg, Daken ; University of Florida, Department of Materials Science and Engineering Williams, Jon; University of Mississippi, Chemistry and Biochemistry Abboud, Khalil; University of Florida, Department of Chemistry Xue, Jiangeng; University of Florida, Department of Materials Science and Engineering Hammer, Nathan; University of Mississippi, Chemistry & Biochemistry Castellano, Ronald; University of Florida, Department of Chemistry Watkins, Davita; University of Mississippi, Chemistry and Biochemistry

Tuning the Structural and Spectroscopic Properties of Donor-Acceptor-Donor Oligomers via Mutual X-Bonding, H-Bonding, and π-π Interactions

Asmerom O. Weldeab[a], April Steen[b], Daken J. Starkenburg[c], Jon Steven Dal Williams[b], Khalil A. Abboud[a], Jiangeng Xue[c], Nathan I. Hammer[b], Ronald K. Castellano[a], and Davita L. Watkins[b]**

[a]Department of Chemistry, University of Florida, Gainesville, FL 32611, USA

[b]Department of Chemistry and Biochemistry, University of Mississippi, University, MS 38677, USA

[c]Department of Materials Science and Engineering, University of Florida, Gainesville, FL 32611, USA

ABSTRACT. Presented are design strategies towards hierarchically assembling a C_2-symmetric π-conjugated oligomer (**DAD-XB-Boc**) based on a donor-acceptor-donor motif through hydrogen bonding (HB), halogen bonding (XB), and π-stacking interactions. Upon co-crystallization with tetrafluoro-1,4-diiodobenzene (**TFDIB**), single crystal X-ray analysis reveals highly directional XB induced 2D assemblies which further organize via π-π interactions. Crystal photoluminescence

(PL) analysis indicates that the co-crystal exhibits a red shift in its PL spectrum with enhanced intensity compared to the mono-crystal. Pyrolytic cleavage and removal of the *t*-butyloxycarbonyl (Boc) groups of **DAD-XB-Boc** exposes complementary hydrogen bonding sites; the H-bonding capability of **DAD-XB-NH** is evident from thermal gravimetric analysis (TGA) and infrared (IR) spectroscopy. Overall, the data shows that both halogen and hydrogen bonding can be used together with π-stacking interactions to enhance the solid-state properties of DAD oligomers essential for optoelectronic device applications. Ongoing work seeks to use such supramolecular approaches to control the nanoscale to microscale arrangement of molecules in thin films and increase device efficiency (i.e., charge mobility).

INTRODUCTION

The operational efficiency of optoelectronic devices such as organic photovoltaic cells (OPVs) and organic field effect transistors (OFETs) depends not only on the molecular structures of the π-conjugated organic molecules but also critically on their solid-state arrangements.[1] Indeed, tremendous strides have been made through synthesis and computation to achieve π-conjugated molecules with desirable intrinsic optical, electronic, and chemical reactivity profiles.[2-6] Of ongoing interest is the use synergetic noncovalent interactions to influence the nanoscale arrangement of otherwise attractive π-systems in crystals and thin films to ultimately enhance device efficiency. Along these lines, we recently exploited *hydrogen bonding* (HB) and π-π stacking interactions to program multidimensional assemblies of phthalhydrazide-functionalized quaterthiophenes in bulk heterojunction OPVs.[7, 8] Photovoltaic devices made from blends of the HB-capable donor molecules with C_{60} as the electron acceptor exhibited a two- to three-fold enhancement in power conversion efficiency relative to non-HB-capable comparators. These

results highlight the effectiveness of complementing π-interactions with additional directional noncovalent interactions to realize more advantageous semiconductor solid-state ordering.

Although HB interactions have gained significant traction for controlling organic semiconductor thin film morphology, hardly scrutinized to date are *halogen bonding* (XB) interactions despite their functional similarity and robustness in crystal engineering.[9-11] Halogen bonds are noncovalent interactions between Lewis acidic halogen atoms (i.e., the XB donor) and electron-pair-donating heteroatoms (i.e., the XB acceptor).[12, 13] In XB, the presence of a region of positive electrostatic potential (i.e., the σ-hole) on the outermost surface of a halogen atom[14, 15] affords a highly directional interaction with electron donating heteroatoms such as oxygen, sulfur, and/or nitrogen. XB interaction energies can be comparable to and even higher than HB interactions, making them useful for the design and construction of stable molecular complexes.[16, 17] Despite the functional similarity between HB and XB, the latter has yet to be broadly deployed for organic semiconductor solid-state applications.

In recent experimental and computational model studies using organic semiconductor building blocks, we examined the combined effects of XB and π-π interactions on the formation of stable supramolecular architectures.[18] Halogen bond driven assemblies between pyridyl thiophene (**Pyr-T**)—a π-conjugated building block equipped with an XB acceptor—and iodopentafluorobenzene (**IPFB**) revealed XB and π-π stacking interactions of similar magnitude (Fig. 1a). Experimental results (i.e., spectroscopic, crystallographic, and thermal data) provided direct evidence of the interplay between XB and π-stacking interactions, while density functional theory (DFT) computations demonstrated that XB and π-stacking were principally responsible for the observed assembly. This investigation provided preliminary guidance towards applying XB for organizing more sophisticated π-conjugated frameworks.

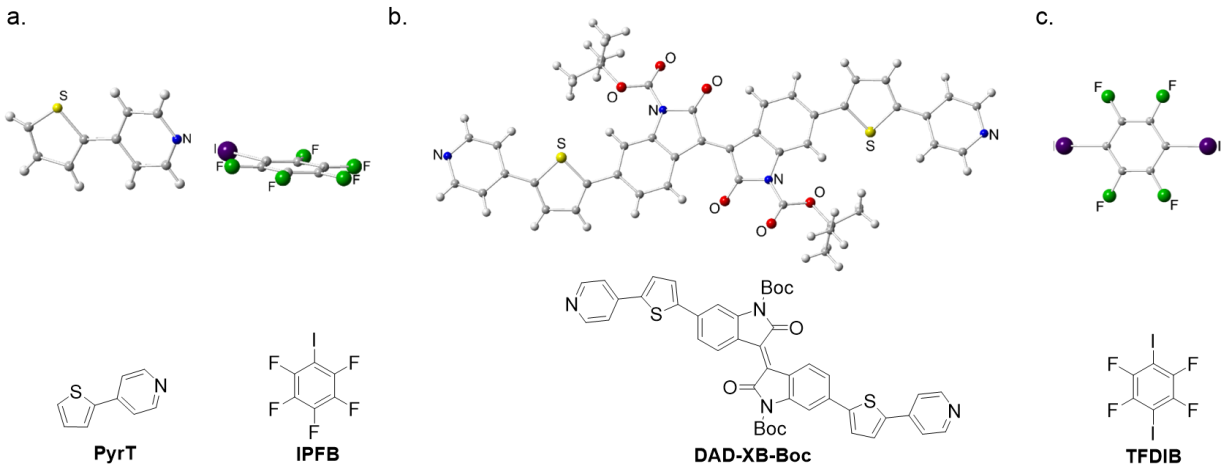

Figure 1. Molecular structures of interest: a) X-ray crystal structure of previously studied co-crystal **PyrT_IPFB**;[18] b) single **DAD-XB-Boc** molecule (XB acceptor) and c) single **TFDIB** molecule (XB donor) abstracted from the crystal. Molecular structures of **PyrT**, **IPFB**, **DAD-XB-Boc**, and **TFDIB** are also shown.

Here we extend the pyridyl XB motif to a C_2-symmetric π-conjugated oligomer, **DAD-XB-Boc**, to examine the consequences of synergetic XB and π-stacking interactions on its solid-state structure and optical properties (Fig. 1b). The molecule features the Donor-Acceptor-Donor (**DAD**) design,[19, 20] a popular one for securing useful absorption and emission properties for various applications. An additional design aspect is use of thermally cleavable solubilizing groups (i.e., Boc) on the lactam ring of the acceptor (isoindigo) core, which, upon removal, introduce a third noncovalent interaction, HB. **DAD-XB-Boc** could therefore serve as an application-relevant model system for understanding the interplay of XB, HB, and π-π stacking interactions on solid-state structure and optical properties. Described here is co-crystal formation from **DAD-XB-Boc** and tetrafluoro-1,4-diiodobenzene **TFDIB** (Fig. 1); the **DAD-XB-Boc_TFDIB** crystal reveals the presence of XB and π-π stacking which has consequences on solid-state optical properties.

Thermal cleavage of Boc and exposure of the NH groups of isoindigo could then be performed (verified by thermal gravimetric analysis (TGA) and infrared (IR) spectroscopy) to provide an organic semiconductor whose 3D solid-state arrangement is guided by synergetic HB and π-π stacking interactions. In ongoing work the synergism between all three interactions is being studied in the context of device-relevant organic semiconductors.

EXPERIMENTAL SECTION

Reagents and solvents were purchased from commercial sources and used without further purification unless otherwise specified. Solid-state IR spectra were recorded using a Perkin Elmer Spectrum One FT-IR spectrophotometer. Additional synthetic details, a summary of theoretical calculations, structural figures, and X-ray crystallographic tables containing bond distances and angles can be found in the SI.

Thermogravimetric Analysis (TGA). Using 3 mg of each sample (**DAD-XB-Boc** and **DAD-XB-NH**), TGA measurements were performed on a TA Instruments Q5000 (platinum pan, room temperature to 600 °C, ramp rate = 20 °C/min under N_2 atmosphere) and analyzed using Universal Analysis 2000 4.4A software.

TGA Coupled with Infrared Spectroscopy. TGA was carried out using an EXSTAR 6000 SII coupled with a Cary 660 FT-IR (Agilent Technologies) to determine the presence of carbonates and identify gases evolved when the samples of **DAD-XB-Boc** were heated. Briefly, approximately 16 mg of sample was placed in a ceramic cup and heated from 30 °C to 1100 °C at a rate of 10 °C per minute. Evolved gases were carried by high-purity nitrogen through silicone tubing to a gas cell located in the FT-IR beam path. FT-IR spectra were collected every 20 s (average of eight scans) from 400 to 6000 cm^{-1} at a 4 cm^{-1} interval.

X-ray Crystallography. X-ray intensity data were collected at 100 K on a Bruker DUO diffractometer using MoKα radiation (λ = 0.71073 Å) and an APEXII CCD area detector. Raw data frames were read by the program SAINT[1] and integrated using 3D profiling algorithms. The resulting data were reduced to produce hkl reflections and their intensities and estimated standard deviations. The data were corrected for Lorentz and polarization effects and numerical absorption corrections were applied based on indexed and measured faces. The structures were solved and refined in *SHELXTL2014*, using full-matrix least-squares refinement. The non-H atoms were refined with anisotropic thermal parameters and all of the H atoms were calculated in idealized positions and refined riding on their parent atoms. Crystal data and structure refinement parameters for all compounds are given in the SI. The single X-ray crystal structure of the mono-crystal and co-crystal CCDC number are 1813579 and 1813580, respectively.

Theoretical Calculations. The final ground state geometries and frontier orbital energies were obtained from DFT calculations at the B3LYP/6-31G* level as implemented in Gaussian 09.[21] Frequency calculations were also performed to verify the geometries as energy minima. Molecular orbital plots were made using the Visual Molecular Dynamics (VMD) software from the Gaussian output files.[22]

Spectroscopic Methods. Solution absorption spectra were recorded on a Cary 100 Bio UV-Visible spectrophotometer using 1 cm quartz cells. Solution emission spectra were recorded on a Photon Technology International (PTI) fluorimeter and collected 90° relative to the excitation beam. The solid-state absorption of all the dyes was also measured by diffuse reflectance spectroscopy. Solid-state absorbance (diffuse reflectance) of the mono-crystal and co-crystal were taken by directing the emission of a Xenon arc lamp on the sample using a solarization resistant fiber optic cable. The sample was placed inside an IC2 integrating sphere from Stellar Net Inc. and

the fiber optic was connected to the illuminator input port. A second fiber optic cable was used to collect light from inside the integrating sphere and direct it to an OceanOptics USB2000 spectrometer. The collected spectrum was compared to a standard composed of Spectralon® in order to determine the percent reflectivity of the sample.[23] Mono-crystal and co-crystal fluorescence spectra were obtained using a Nikon TE2000U inverted microscope with charge coupled device (CCD) detection and using a pulsed 405 nm picosecond diode laser for excitation. Excited state lifetime data was obtained using the inverted microscope, the pulsed diode laser, and a PicoQuant PMD series single photon avalanche diode with a 50 picosecond timing resolution. These values obtained using time correlated single photon counting were then fit to a single exponential decay function to determine the excited state lifetimes. For the co-crystal lifetime, the uncertainty in the fit of the curve is 0.005 ns. For the mono-crystal lifetime, the uncertainty is 0.0004 ns. For **DAD-XB-NH**, the lifetime uncertainty is 0.001 ns.

Powder X-ray Diffraction. Powder XRD measurements were performed with a Panalytical XPert Powder Diffractometer using a copper source with a corresponding X-ray emission wavelength of 1.5406 Å. The instrument was used to measure 2θ angles from 5 degrees to 70 degrees.

RESULTS AND DISCUSSION

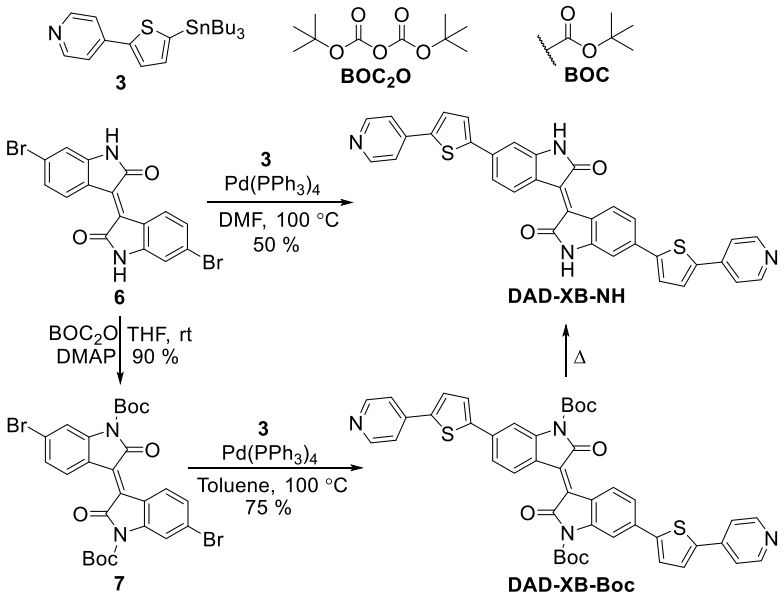

Scheme 1. Synthesis of **DAD-XB-Boc** and **DAD-XB-NH**

Design and Synthesis. The halogen bond acceptor, **DAD-XB-Boc**, features a Donor-Acceptor-Donor (DAD) construction which provides a narrow energy gap and visible light absorption.[19, 20, 24, 25] Isoindigo is incorporated as an electron acceptor (A) unit at the center of the molecule,[26] while thiophenes are used as electron donors (D) and capped with pyridine groups as XB acceptors. **TFDIB** has been selected as the XB donor as the fluorine substituents provide an inductive effect that increases the magnitude of σ-hole on the halogen atom; in turn, increasing the strength of the XB interaction.[13, 27] Upon co-crystallization, interaction between the pyridyl nitrogens (of **DAD-XB-Boc**) and iodine groups (of **TFDIB**) are expected to direct linear self-association along the π-system's long molecular axis.

Further within the design, Boc has been installed as a solubilizing group as it is amenable to pyrolytic cleavage and the unmasking of the lactam HB functionality.[28] It is well established that the lactam rings of the isoindigo can form ordered arrangements driven by HB.[28-31] The removal

of Boc is expected to relieve the insulation provided by the solubilizing group, promote planarity, and enhance π-π interactions. The byproducts of thermal cleavage of the Boc groups, CO_2 and isobutene, are both gases and hence can escape the system without introducing impurities.

The syntheses of **DAD-XB-Boc** and **DAD-XB-NH** were achieved as shown in Scheme 1. Intermediates **3**, **6**, and **7** were synthesized following literature procedures.[18, 32-34] Ultimately, Stille coupling between *t*-butyloxycarbonyl (Boc)-protected isoindigo (**7**) and stannylated thiophene-pyridine (**3**) afforded the final target **DAD-XB-Boc** in 75 % yield. The structural integrity of **DAD-XB-Boc** was confirmed by ^{1}H NMR, ^{13}C NMR, and high resolution mass spectrometry (HRMS). **DAD-XB-NH** was also obtained in good yields following a similar route using compound **6** as a starting material. Its structure was confirmed by ^{1}H NMR and high resolution mass spectrometry (HRMS). ^{13}C NMR analysis was not successful due to the very poor solubility of the compound.

Table 1. Crystallographic information and selected structural features

	DAD-XB-Boc	**DAD-XB-Boc_TFDIB**	**PyrT_IPFB**[18]
Formula	C_{46} H_{38} Cl_6 N_4 O_6 S_2	C_{58} H_{52} F_4 I_2 N_4 O_8 S_2	C_{15} H_7 F_5 I N S
M (g/mol)	1019.62	1326.96	455.18
Temperature (K)	100.0	100.0	100.0
Space group	Pī	Pī	$P2_1/n$
a (Å)	8.2494(3)	8.1917(4)	8.7694(5)
b (Å)	9.3069(4)	9.5688(5)	7.5097(4)
c (Å)	15.1499(7)	18.0523(10)	22.9574(13)
α (deg)	87.1718	100.6726	90.00
β (deg)	78.7559	91.6388	91.7573
γ (deg)	77.6043	104.9351	90.00
V (Å^3)	1114.2	1339.2	1511.2
Z	1	1	4
R factor (%)	3.61	2.51	1.58

Co-crystal Growth and Analysis. Diffraction quality single crystals of **DAD-XB-Boc** and co-crystal **DAD-XB-Boc_TFDIB** were obtained by vapor diffusion methods. Crystals from **DAD-XB-NH** could not be obtained due to the insolubility of the material. Comparative analysis of the crystal structures of **DAD-XB-Boc** and **DAD-XB-Boc_TFDIB** reveals the influence of introduced XB interactions on the packing structure. A summary of the crystallographic data is provided in Table 1.

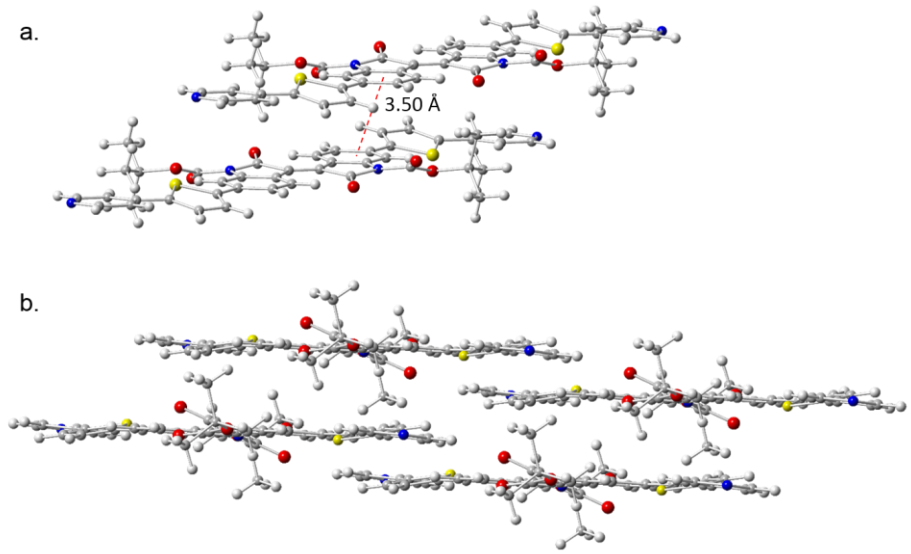

Figure 2. X-ray crystal structure of the mono-crystal of **DAD-XB-Boc** and its co-facial π-stacking arrangement. a) π–π stacking interactions between molecules; b) packing structure highlighting additional nearest neighbor contacts. Dashed lines show the interplanar distances measured using the centroid of the neighboring ring (Fig. S3).

Mono-crystals of **DAD-XB-Boc** exhibit a triclinic structure with a $P\bar{1}$ space group (Fig. 2, Table 1). The **DAD-XB-Boc** molecules pack into a two-dimensional array where the conjugated backbones are twisted (12–15°) at the thiophene moiety (Fig. S1). Face-to-face π–π orientations between molecules exhibit an interplanar distance of 3.50 Å (Fig. 2a). The length of **DAD-XB-**

Boc enables each molecule to participate in interactions with up to seven other molecules. These nearest neighbor contacts which are found between the longest molecular axis of the nearest molecules are as short as 5.73 Å (39.7°; Fig. S3) and indicate a very compressed molecular structure and strong intermolecular interactions (Fig. 2b).

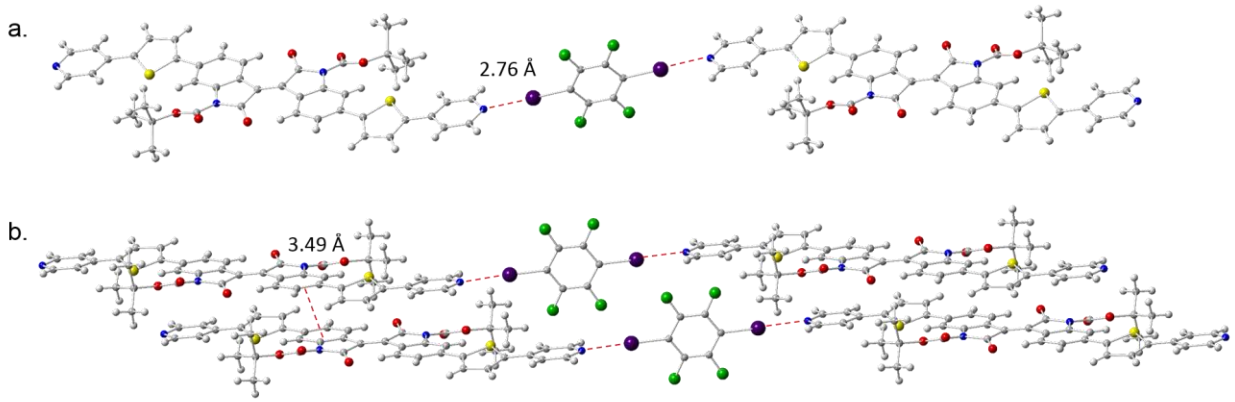

Figure 3. X-ray crystal structure of the complex of **DAD-XB-Boc** and **TFDIB**: a) ditopic XB interaction (red dotted line); b) π–π stacking interactions between **DAD-XB-Boc** molecules. Dashed lines show the interplanar distances measured using the centroid of the neighboring ring (Fig. S4).

Co-crystal **DAD-XB-Boc_TFDIB** was formed as a 2:1 ratio of **DAD-XB-Boc** and **TFDIB**; the crystal exhibits a triclinic structure with a $P\bar{1}$ space group (Fig. 3). Unlike the 1:1 assembly of its truncated precursor (i.e., **Pyr-T** with **IPFB**),[35] the ditopic XB interactions afford infinite linear chains in which the N···I–C angle is 175.3° and the N···I distance is 2.73 Å corresponding to a 22.7 % shortening relative to the total van der Waals radii of nitrogen and iodine (Fig. 3a). These XB interactions are similar to those observed in **PyrT_IPFB** (2.76 Å, 21.8 %). The XB donor and acceptor π-surfaces adopt a perpendicular arrangement (~ 85.2° between the molecular planes) similar to the C_s structure of the **PyrT_IPFB** complex. Interestingly, the interplanar π–π stacking

distances within the **DAD-XB-Boc_TFDIB** co-crystal are smaller (by ~ 0.20 Å) than those in **PyrT_IPFB** despite the presence of the bulky Boc groups at the isoindigo core. However, unlike **PyrT_IPFB**, pairwise **DAD-XB-Boc_TFDIB** molecules exhibit a slipped-stack arrangement along the *b*-axis and pack closely (3.49 Å) along the *a*-axis (Fig. 3b).

The conformation of the XB acceptor backbone essentially remains the same from mono-crystal to co-crystal (Fig. S1). The incorporation of **TFDIB** molecules afford molecular columns (i.e., segregated packing) of **DAD-XB-Boc** and **TFDIB** within the co-crystal. The nearest neighbor contacts along the molecular axis of the **DAD-XB-Boc** molecule was found to be reduced from seven to four with the shortest distance between molecules being 5.68 Å (39.4°; Fig. S4). Additional nearest neighbor contacts, such as F···H (2.53 Å) and C=O···H (2.32 Å), contribute to planarity of the conjugated **DAD-XB-Boc** backbone as well as slightly shorter intermolecular distances (Fig. S4).

Photophysical Analysis. The photophysical properties of **DAD-XB-Boc** were studied in order to understand perturbations from the molecular level through to the solid-state with and without XB interactions. Similar studies have been reported noting that co-crystals based on XB can lead to distinct photophysical changes such as bathochromic shifts and large Stokes shifts attributed to CT transitions and variations in the co-crystal packing structure.[36-39]

Initial studies began with gas phase DFT calculations (B3LYP/6-31G*) to obtain the ground state geometry and electronic structure of the XB acceptor **DAD-XB-Boc** (Fig. 4a). Frequency calculations were also performed to verify the geometries as energy minima. The conformation of the thiophenes with respect to the isoindigo core was initially set based on the X-ray crystal structure of the mono-crystal (**DAD-XB-Boc**).

The π-framework of **DAD-XB-Boc** calculated in the gas-phase is relatively planar with a slight twisting (~ 20°) between adjacent rings (Fig. S1a). Consequently, the planarity of the molecule is significantly enhanced in the solid-state (based on the X-ray crystal analysis) with smaller torsion angles of 15° (thiophene/pyridine), 12° (isoindigo/thiophene), and 0° (between the lactam rings of the isoindigo core unit) (Fig. S1b). Certainly packing interactions are responsible, and interestingly the enhanced planarity observed in the mono-crystal is perfectly conserved in the co-crystal (Fig. S1c).

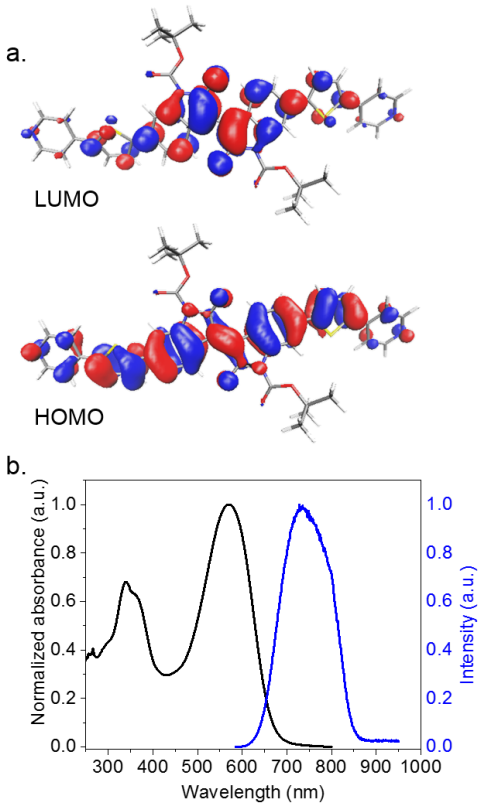

Figure 4. a) HOMO and LUMO orbital density plots of **DAD-XB-Boc** derived from DFT calculations (B3LYP/6-31G*); b) normalized solution phase absorption (black) and emission (blue) profiles for **DAD-XB-Boc** in DMF (20 μM)**.** ($\lambda_{excitation}$ = 570 nm)

The photophysical properties of **DAD-XB-Boc** were also studied by absorption and emission spectroscopy in solution (Fig. 4b). UV-Vis spectroscopy in DMF indicates that **DAD-XB-Boc** possesses two strong absorption bands in both the UV and visible region with a maximum absorption of 570 nm and molecular absorptivity of 37,000 M^{-1} cm^{-1}. Based on previous reports of D-A systems, the high-energy band (344 nm) is attributed to a π-π* transition and the low energy band (570 nm) corresponds to charge transfer that arises due to the push-pull nature of the molecule.[40, 41] The push-pull character is reflected by the gas phase DFT calculations as well (Fig. 4a): the LUMO (–3.23 eV) of **DAD-XB-Boc** is largely localized on the isoindigo acceptor unit while the HOMO (–5.48 eV) is delocalized throughout the π-conjugated backbone (with highest electron density on the electron rich thiophene and benzene units). The narrow optical HOMO–LUMO gap ($\Delta E_{g\text{-}opt}$ = 1.87 eV), calculated from the onset (663 nm) of the solution absorption profile, is also reflected in the observed dark purple color of the compound. A linear (R^2 = 0.999) Beer-Lambert plot is consistent with the compound being fully soluble and showing no aggregation in the concentration range studied (2.5–20 μM) (Fig. S2). Solution absorption profiles of **DAD-XB-NH** were attempted in DMSO (onset = 655 nm, $\Delta E_{g\text{-}opt}$ = 1.89 eV); however, a nonlinear (R^2 = 0.966) Beer-Lambert plot was obtained attesting to the poor solubility of the compound (Fig.S2).

The emission spectrum of **DAD-XB-Boc** in DMF shows a structureless fluorescence band that extends into the near-IR region with a maximum emission wavelength of 736 nm, dictating a large Stokes shift of 166 nm. A shift of such magnitude suggests the presence of conformational changes in the molecule upon excitation from the ground to excited state as well as interactions of the chromophore with the local environment.[40, 42, 43] Such large Stokes shifts are especially important for applications in optoelectronic devices as it minimizes self-quenching.[44] Solution

photophysical studies were not performed in the presence of **TFDIB** as the XB interactions are expected to be weak at these concentrations.

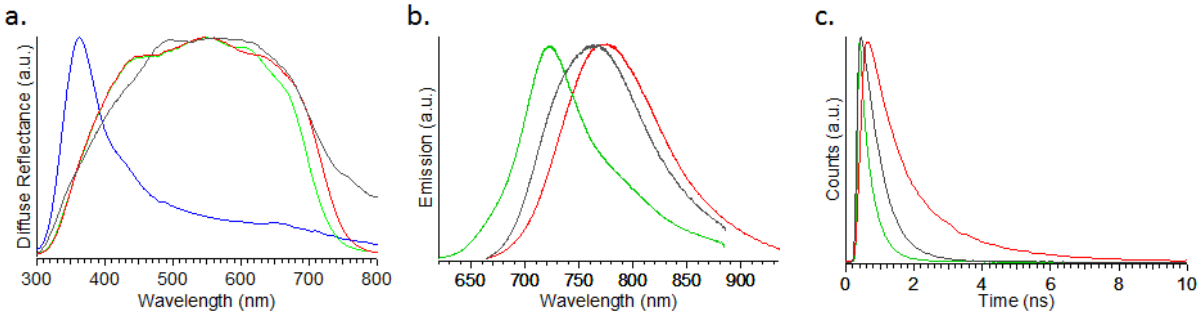

Figure 5. Normalized solid-state absorption (a) spectra for crystals of **DAD-XB-NH** (purple), **DAD-XB-Boc** (green), **DAD-XB-Boc-TFDIB** (red), and **TFDIB** (blue); normalized solid-state emission (b) and excited state PL lifetime (c) measurements for **DAD-XB-NH** (purple), **DAD-XB-Boc** (green) and **DAD-XB-Boc-TFDIB** (red). ($\lambda_{excitation}$ = 405 nm for b and c).

The photophysical analysis was extended to the solid-state, specifically on mono-crystal **DAD-XB-Boc** and co-crystal **DAD-XB-Boc-TFDIB**, in order to understand the effect of halogen bond driven assembly on photophysical properties. Additionally, **DAD-XB-NH** was included for comparative purposes as co-crystallization with **TFDIB** was not achievable. The **DAD-XB-Boc** mono-crystal (Fig. 5a) shows a red-shift of ~ 58 nm (absorption onset = 743 nm, $\Delta E_{g\text{-}opt}$ = 1.67 eV) and significantly broadened absorption when compared to **DAD-XB-Boc** in solution (Fig. S2). This is explained by the enhanced planarity and co-facial π-π stacking observed for the molecules in the solid state.[7, 8, 45-47] The **DAD-XB-Boc-TFDIB** co-crystal exhibits *an additional* red-shift of 21 nm compared to that of the mono-crystal (absorption onset = 763 nm, $\Delta E_{g\text{-}opt}$ = 1.62 eV), potentially speaking to stronger intermolecular interactions between the molecules mediated by both XB and π-π interactions. In comparison to both mono- and co-crystal, **DAD-XB-NH** displays

an absorption onset of 809 nm ($\Delta E_{g\text{-}opt}$ = 1.53 eV). The larger onset value is presumably due to the absence of sterically hindering Boc groups affording greater planarity and π-stacking than that attainable for **DAD-XB-Boc**.

Crystal photoluminescence (PL) analysis (Fig. 5b) shows that the mono-crystal displays an emission spectrum with λ_{em} = 737 nm almost identical to the one in solution. However, the co-crystal reveals a significantly red-shifted emission with λ_{em} = 780 nm. Consistent with this result, excited state PL lifetime measurements reveal that the co-crystal exhibits a four-fold increased lifetime (1.28 ns) when compared to the mono-crystal (0.34 ns). The increase in the excited state PL lifetime as well as the red shift in the emission spectrum could be attributed to an increased rigidity of the system which in turn decreases the non-radiative decay pathways.[48, 49] Photophysical studies with just the XB donor (**TFDIB**) show that the molecule alone is not responsible for the observations. It is, however, evident that the addition of **TFDIB** to form XB leads to an extended π-electron system and affords charge transfer (CT) interactions that change the solid-state spectroscopic properties of **DAD-XB-Boc**.[37, 50, 51] This is supported by a broad, structureless red-shifted absorbance and longer PL lifetime. Additional photophysical studies with **DAD-XB-NH** attest to the implications of XB as **DAD-XB-NH** displays a red-shifted emission (λ_{em} = 763 nm) compared to the mono-crystal but a shorter lifetime (0.61 ns) in comparsion to the co-crystal. In general, the data obtained indicates that the introduction of XB interactions does not disturb the overall solid-state packing of the XB acceptor **DAD-XB-Boc**, but instead enhances rigidity and improves solid-state photophysical properties.

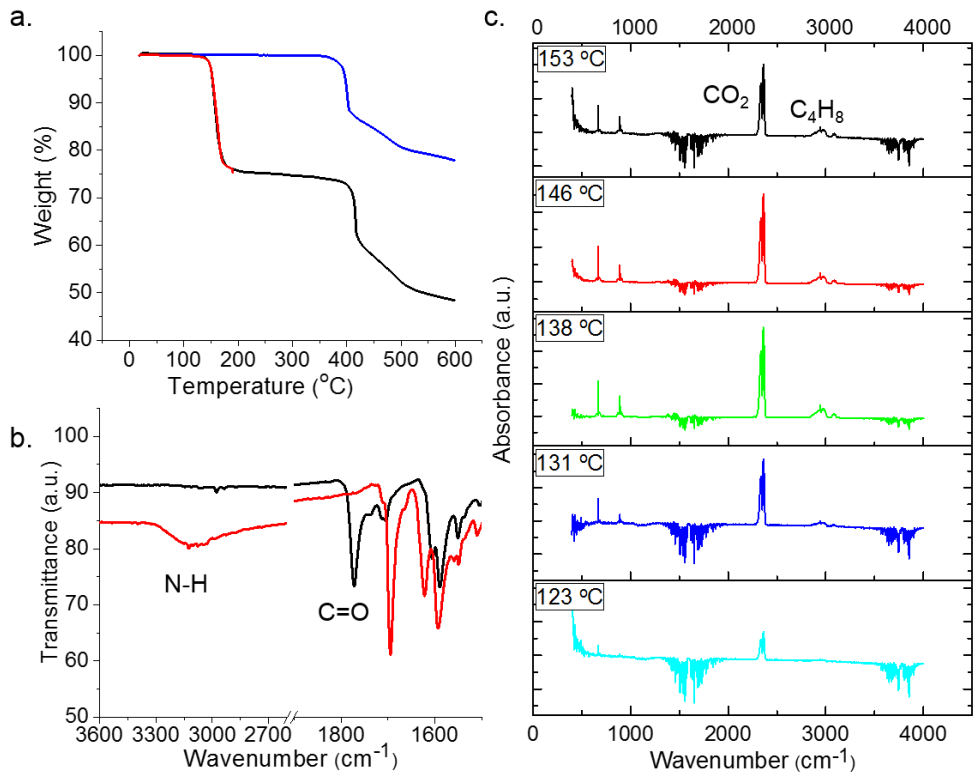

Figure 6. a) TGA analysis: full TGA analysis of **DAD-XB-Boc** (black); TGA analysis where **DAD-XB-Boc** is heated and held at 190 °C (30 min) to generate **DAD-XB-NH** (red); full TGA analysis of synthesized **DAD-XB-NH** (blue); b) powder FT-IR spectra comparison of **DAD-XB-Boc** (black) and pyrolytically obtained **DAD-XB-NH** (red); c) coupled TGA-FTIR spectra to monitor the release of CO_2 and isobutene.

Introduction of Hydrogen Bonding Sites. Due to the difference in solubility between the two components, co-crystallization of **DAD-XB-NH** and **TFDIB** was not achieved. Alternatively, the Boc groups of **DAD-XB-Boc** were cleaved thermally to expose complementary HB sites and the effects of both HB and π–π interactions were evaluated by TGA and FT-IR (Fig. 6). As shown in Fig. 6a, TGA analysis of **DAD-XB-Boc** showed a 24% weight loss at 190 °C, which roughly corresponds to the loss of the Boc groups as CO_2 and isobutene to form **DAD-XB-NH**. This is

further supported by the TGA of the as-synthesized **DAD-XB-NH**, whose curve showed a similar weight loss trend when compared to the pyrolytically obtained **DAD-XB-NH**. Once the Boc groups are removed, the remaining HB capable product remains thermally stable up to ~ 400 °C.

To further confirm the formation of the HB-driven assembly, the IR spectrum of **DAD-XB-Boc** was compared to **DAD-XB-NH** obtained pyrolytically (Fig. 6b). The appearance of a broad band at 3130 cm^{-1} in the IR spectrum of **DAD-XB-NH** corresponding to the NH stretch confirms exposure of the HB sites. A significant change was also observed by IR spectroscopy for the C=O stretch, which shifted from 1772 cm^{-1} in **DAD-XB-Boc** to 1694 cm^{-1} in **DAD-XB-NH**. The C=O and N–H stretch energies are consistent with the formation of intermolecular HB interactions between the carbonyl in the lactam rings of one molecule and NH of an adjacent molecule (N-H···O=C). Similar changes have been reported in Boc protected DPP systems.[30]

The formation and release of CO_2 and isobutene, upon pyrolytic cleavage and removal of the Boc groups from **DAD-XB-Boc**, has also been monitored by TGA-FTIR. As shown in Figure 6c, an increase in the intensity of the peaks at 2352, 2947, 3095 cm^{-1} upon increasing the temperature corresponds to the formation and escape of CO_2 and isobutylene. The data concludes that HB is accessible via thermal cleavage of the Boc groups to yield materials stable up to 400 °C.

Powder XRD was used to verify the crystallinity of the material after thermal treatment. Comparing X-ray spectra data of **DAD-XB-Boc** (Fig. S5, black trace) to that of the post treated product (Fig. S5, blue trace), the material obtained is indeed crystalline as indicated by new peaks corresponding to those present in **DAD-XB-NH** (Fig. S5, red trace). Furthermore, the XRD data shows that the compound crystal packing has changed with the thermal cleavage as noted by the absence of peaks below 9 degrees 2θ as well as the presence of new diffraction peaks at 15, 18, 21 and 26 degrees 2θ. Given the processing differences between thermally cleaved and pre-prepared

DAD-XB-NH, future studies are aimed towards elucidating the different packing structures observed. Combined with thermal and spectroscopic analysis, these results provide evidence for morphological and crystalline changes with thermal treatment to **DAD-XB-Boc** and demonstrates the subsequent acquisition of **DAD-XB-NH** implemented in the design strategy.

CONCLUSION

An application-relevant model system for understanding the interplay of noncovalent interactions on solid-state structure and optical properties was successfully synthesized and its assemblies were studied. Crystal structure analysis indicates that strong π−π interactions between **DAD-XB-Boc** molecules are the main driving force for self-assembly in the mono-crystal. When **TFDIB** is incorporated, variations to the solid-state order arise in which infinite chains are afforded via XB. The interplay of XB and π−π interactions results in co-crystals consisting of segregated molecular columns of both the XB donor and acceptor. There is a slipped stack arrangement between XB chains that is beneficial to the overlap between the **DAD-XB-Boc** molecules (Fig. S4).[1, 52] The XB acceptor molecules have a slightly shorter intermolecular distance (< 1 Å) between nearest neighbors implying that although the number of molecular contacts have changed, the strong π−π interactions are still essential to the assembly. Analysis via absorbance and photoluminescence spectroscopy highlights the significance of noncovalent interactions in enhancing the properties of optoelectronic materials. As a CT interaction,[50, 51, 53, 54] XB induces an intermolecular packing configuration that slightly differs from that of the mono-crystal but strongly manifests in the photophysical properties.

Critical to the design is the thermal cleavage of the Boc groups of **DAD-XB-Boc** that induces HB via N−H···O=C interactions at the isoindigo core. Complementary HB and π−π

interactions are evident via TGA-FTIR in which a decomposition of ~400 °C is observed. Powder XRD was used to verify the accessibility of the **DAD-XB-NH** derivative from **DAD-XB-Boc** and confirmed the crystallinity of the material after thermal treatment. Due to limitations in solubility, direct evidence of all three noncovalent interactions was not attainable; however, research is underway to investigate the synergistic effects of HB, XB, and π–π interactions on DAD molecular structure, packing, and thin film optical properties. In summary, the work provides an example of a promising organic semiconducting material in which HB, XB, and π–π interactions have been used in a combined fashion to influence solid-state ordering and photophysical properties.

Conflicts of Interest

There are no conflicts to declare.

ASSOCIATED CONTENT

Supporting Information

Electronic Supplementary Information (ESI) available: crystallographic data, details of the thermal analysis, details of the theoretical calculations, ^{1}H NMR spectra, and supplementary results. See DOI: 10.1039/x0xx00000x

AUTHOR INFORMATION

***Corresponding Authors**

castellano@chem.ufl.edu

dwatkins@olemiss.edu

Author Contributions

The manuscript was written through contributions of all authors. All authors have given approval to the final version of the manuscript.

ACKNOWLEDGMENT

D.L.W. and J.S.D.W. appreciate financial support of this work from the University of Mississippi for Laboratory Start-up Funds. R.K.C. and A.O.W. are grateful for financial support from the National Science Foundation (CHE-1507561). A.E.S. and N.I.H. acknowledge support from the National Science Foundation under Grant Number OIA-1539035. KAA wishes to acknowledge the National Science Foundation and the University of Florida for funding of the purchase of the X-ray equipment. We thank the University of Florida High-Performance Computing Center for providing computational resources.

REFERENCES

1. H. Bässler and A. Köhler, in *Unimolecular and Supramolecular Electronics I*, ed. R. M. Metzger, Springer Berlin Heidelberg, 2012, vol. 312, ch. 218, pp. 1-65.
2. M. Jeffries-El, B. M. Kobilka and B. J. Hale, *Macromolecules*, 2014, **47**, 7253-7271.
3. K. Takimiya, M. Nakano, H. Sugino and I. Osaka, *Synth. Met.*, 2016, **217**, 68-78.
4. T. Aytun, L. Barreda, A. Ruiz-Carretero, J. A. Lehrman and S. I. Stupp, *Chem. Mater.*, 2015, **27**, 1201-1209.
5. S. J. Kang, S. Ahn, J. B. Kim, C. Schenck, A. M. Hiszpanski, S. Oh, T. Schiros, Y.-L. Loo and C. Nuckolls, *J. Am. Chem. Soc.*, 2013, **135**, 2207-2212.
6. J. D. Tovar, *Acc. Chem. Res.*, 2013, **46**, 1527-1537.
7. N. T. Shewmon, D. L. Watkins, J. F. Galindo, R. B. Zerdan, J. Chen, J. Keum, A. E. Roitberg, J. Xue and R. K. Castellano, *Adv. Funct. Mater.*, 2015, **25**, 5166-5177.
8. B. M. Schulze, N. T. Shewmon, J. Zhang, D. L. Watkins, J. P. Mudrick, W. Cao, R. Bou Zerdan, A. J. Quartararo, I. Ghiviriga, J. Xue and R. K. Castellano, *Journal of Materials Chemistry A*, 2014, **2**, 1541-1549.
9. G. Berger, J. Soubhye and F. Meyer, *Polymer Chemistry*, 2015, **6**, 3559-3580.
10. A. Mukherjee, S. Tothadi and G. R. Desiraju, *Acc. Chem. Res.*, 2014, **47**, 2514-2524.

11. L. P. Wolters and F. M. Bickelhaupt, *ChemistryOpen*, 2012, **1**, 96-105.
12. L. C. Gilday, S. W. Robinson, T. A. Barendt, M. J. Langton, B. R. Mullaney and P. D. Beer, *Chem. Rev.*, 2015, **115**, 7118-7195.
13. G. Cavallo, P. Metrangolo, R. Milani, T. Pilati, A. Priimagi, G. Resnati and G. Terraneo, *Chem. Rev.*, 2016, **116**, 2478-2601.
14. K. Dyduch, M. P. Mitoraj and A. Michalak, *J. Mol. Model.*, 2013, **19**, 2747-2758.
15. F. Meyer and P. Dubois, *CrystEngComm*, 2013, **15**, 3058-3071.
16. A. R. Voth, F. A. Hays and P. S. Ho, *Proceedings of the National Academy of Sciences*, 2007, **104**, 6188-6193.
17. T. L. Ellington, P. L. Reves, B. L. Simms, J. L. Wilson, D. L. Watkins, G. S. Tschumper and N. I. Hammer, *ChemPhysChem*, 2017, **18**, 1267-1273.
18. J. Wilson, J. S. Dal Williams, C. Petkovsek, P. Reves, J. W. Jurss, N. I. Hammer, G. S. Tschumper and D. L. Watkins, *RSC Advances*, 2015, **5**, 82544-82548.
19. H. Ouchi, X. Lin, T. Kizaki, D. D. Prabhu, F. Silly, T. Kajitani, T. Fukushima, K.-i. Nakayama and S. Yagai, *Chem. Commun.*, 2016, **52**, 7874-7877.
20. S. R. Marder, *Chem. Commun.*, 2006, DOI: 10.1039/B512646K, 131-134.
21. M. J. Frisch, G. W. Trucks, H. B. Schlegel, G. E. Scuseria, M. A. Robb, J. R. Cheeseman, G. Scalmani, V. Barone, B. Mennucci, G. A. Petersson, H. Nakatsuji, M. Caricato, X. Li, H. P. Hratchian, A. F. Izmaylov, J. Bloino, G. Zheng, J. L. Sonnenberg, M. Hada, M. Ehara, K. Toyota, R. Fukuda, J. Hasegawa, M. Ishida, T. Nakajima, Y. Honda, O. Kitao, H. Nakai, T. Vreven, J. A. Montgomery Jr., J. E. Peralta, F. Ogliaro, M. J. Bearpark, J. Heyd, E. N. Brothers, K. N. Kudin, V. N. Staroverov, R. Kobayashi, J. Normand, K. Raghavachari, A. P. Rendell, J. C. Burant, S. S. Iyengar, J. Tomasi, M. Cossi, N. Rega, N. J. Millam, M. Klene, J. E. Knox, J. B. Cross, V. Bakken, C. Adamo, J. Jaramillo, R. Gomperts, R. E. Stratmann, O. Yazyev, A. J. Austin, R. Cammi, C. Pomelli, J. W. Ochterski, R. L. Martin, K. Morokuma, V. G. Zakrzewski, G. A. Voth, P. Salvador, J. J. Dannenberg, S. Dapprich, A. D. Daniels, Ö. Farkas, J. B. Foresman, J. V. Ortiz, J. Cioslowski and D. J. Fox, *Journal*, 2009.
22. W. Humphrey, A. Dalke and K. Schulten, *J Mol Graph*, 1996, **14**, 33-38, 27-38.
23. G. E. Tyson, K. Tokmic, C. S. Oian, D. Rabinovich, H. U. Valle, T. K. Hollis, J. T. Kelly, K. A. Cuellar, L. E. McNamara, N. I. Hammer, C. E. Webster, A. G. Oliver and M. Zhang, *Dalton Transactions*, 2015, **44**, 14475-14482.
24. Z. Cai, Y. Guo, S. Yang, Q. Peng, H. Luo, Z. Liu, G. Zhang, Y. Liu and D. Zhang, *Chem. Mater.*, 2013, **25**, 471-478.
25. B. Carsten, J. M. Szarko, H. J. Son, W. Wang, L. Lu, F. He, B. S. Rolczynski, S. J. Lou, L. X. Chen and L. Yu, *J. Am. Chem. Soc.*, 2011, **133**, 20468-20475.
26. J. D. Yuen and F. Wudl, *Energy & Environmental Science*, 2013, **6**, 392-406.
27. P. Politzer, J. S. Murray and T. Clark, *PCCP*, 2013, **15**, 11178-11189.
28. C. Liu, S. Dong, P. Cai, P. Liu, S. Liu, J. Chen, F. Liu, L. Ying, T. P. Russell, F. Huang and Y. Cao, *ACS Applied Materials & Interfaces*, 2015, **7**, 9038-9051.
29. F. Bruni, M. Sassi, M. Campione, U. Giovanella, R. Ruffo, S. Luzzati, F. Meinardi, L. Beverina and S. Brovelli, *Adv. Funct. Mater.*, 2014, **24**, 7410-7419.
30. Y. Suna, J.-i. Nishida, Y. Fujisaki and Y. Yamashita, *Org. Lett.*, 2012, **14**, 3356-3359.
31. B. Sun, W. Hong, H. Aziz and Y. Li, *J. Mater. Chem.*, 2012, **22**, 18950-18955.
32. E. C. Constable, C. E. Housecroft, M. Neuburger and C. X. Schmitt, *Polyhedron*, 2006, **25**, 1844-1863.

33. J. Mei, K. R. Graham, R. Stalder and J. R. Reynolds, *Organic Letters*, 2010, **12**, 660-663.
34. M. Shaker, B. Park, J.-H. Lee, W. kim, C. K. Trinh, H.-J. Lee, J. w. Choi, H. Kim, K. Lee and J.-S. Lee, *RSC Advances*, 2017, **7**, 16302-16310.
35. J. Wilson, J. Williams, C. Petkovsek, P. Reves, J. W. Jurss, N. I. Hammer, G. S. Tschumper and D. Watkins, *RSC Advances*, 2015, **DOI: 10.1039/c5ra16680b**.
36. R. Liu, Y. J. Gao and W. J. Jin, *Acta Crystallographica Section B*, 2017, **73**, 247-254.
37. W. Zhu, R. Zheng, Y. Zhen, Z. Yu, H. Dong, H. Fu, Q. Shi and W. Hu, *J. Am. Chem. Soc.*, 2015, **137**, 11038-11046.
38. D. Yan, A. Delori, G. O. Lloyd, T. Friščić, G. M. Day, W. Jones, J. Lu, M. Wei, D. G. Evans and X. Duan, *Angew. Chem. Int. Ed.*, 2011, **50**, 12483-12486.
39. O. Bolton, K. Lee, H.-J. Kim, K. Y. Lin and J. Kim, *Nature Chemistry*, 2011, **3**, 205.
40. R. R. San Juan, A.-J. Payne, G. C. Welch and A. a. F. Eftaiha, *Dyes and Pigments*, 2016, **132**, 369-377.
41. R. Stalder, J. Mei and J. R. Reynolds, *Macromolecules*, 2010, **43**, 8348-8352.
42. S. Faraji and A. I. Krylov, *J. Phys. Chem. B*, 2015, **119**, 13052-13062.
43. B. Souharce, C. J. Kudla, M. Forster, J. Steiger, R. Anselmann, H. Thiem and U. Scherf, *Macromol. Rapid Commun.*, 2009, **30**, 1258-1262.
44. A. Casey, R. S. Ashraf, Z. Fei and M. Heeney, *Macromolecules*, 2014, **47**, 2279-2288.
45. M. Grell, D. D. C. Bradley, G. Ungar, J. Hill and K. S. Whitehead, *Macromolecules*, 1999, **32**, 5810-5817.
46. S. Steinberger, A. Mishra, E. Reinold, J. Levichkov, C. Uhrich, M. Pfeiffer and P. Bauerle, *Chem. Commun.*, 2011, **47**, 1982-1984.
47. R. Fitzner, E. Reinold, A. Mishra, E. Mena-Osteritz, H. Ziehlke, C. Körner, K. Leo, M. Riede, M. Weil, O. Tsaryova, A. Weiß, C. Uhrich, M. Pfeiffer and P. Bäuerle, *Adv. Funct. Mater.*, 2011, **21**, 897-910.
48. V. V. Sivchik, A. I. Solomatina, Y.-T. Chen, A. J. Karttunen, S. P. Tunik, P.-T. Chou and I. O. Koshevoy, *Angew. Chem. Int. Ed.*, 2015, **54**, 14057-14060.
49. D. Yan, D.-K. Bučar, A. Delori, B. Patel, G. O. Lloyd, W. Jones and X. Duan, *Chemistry – A European Journal*, 2013, **19**, 8213-8219.
50. R. B. Walsh, C. W. Padgett, P. Metrangolo, G. Resnati, T. W. Hanks and W. T. Pennington, *Crystal Growth & Design*, 2001, **1**, 165-175.
51. A. C. B. Lucassen, A. Karton, G. Leitus, L. J. W. Shimon, J. M. L. Martin and M. E. van der Boom, *Crystal Growth & Design*, 2007, **7**, 386-392.
52. V. Coropceanu, J. Cornil, D. A. da Silva Filho, Y. Olivier, R. Silbey and J.-L. Brédas, *Chem. Rev.*, 2007, **107**, 926-952.
53. S. V. Rosokha, I. S. Neretin, T. Y. Rosokha, J. Hecht and J. K. Kochi, *Heteroat. Chem*, 2006, **17**, 449-459.
54. P. Politzer, J. S. Murray and T. Clark, *PCCP*, 2010, **12**, 7748-7757.

Table of Contents Graphic and Synopsis

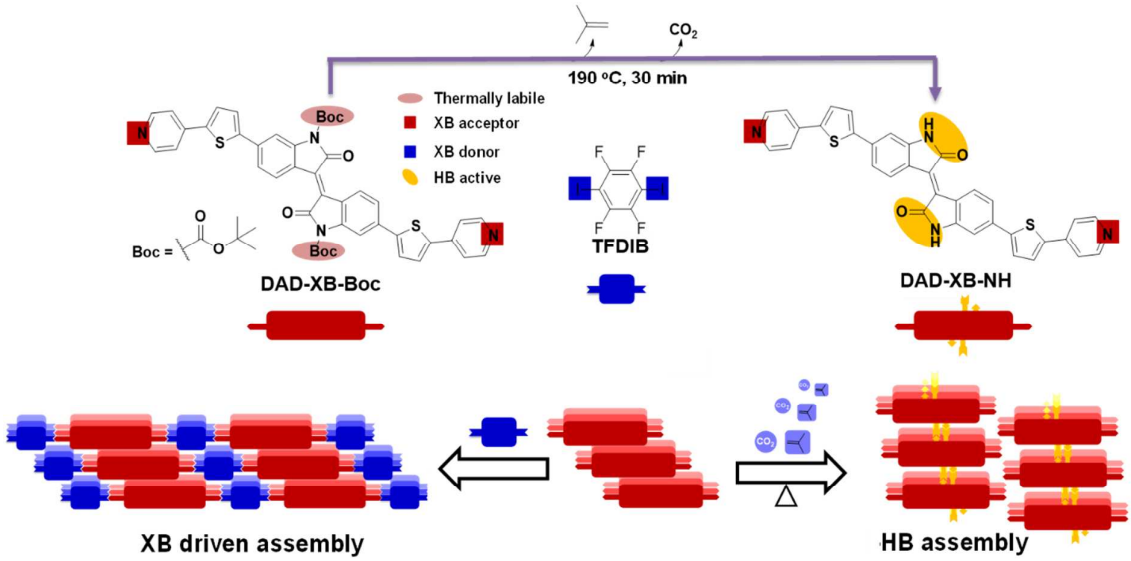

Presented are design principles for the combinatory usage of HB, XB, and π–π interactions to enhance solid-state properties essential for optoelectronic device application.